On the initiation of blow-out from cooktop burner jets: A simplified energy-based description for the onset of laminar flame extinction in premixed hydrogen-enriched natural gas (HENG) systems

Daniel R. Jones[1] and Charles W. Dunnill[1*]

[1]Energy Safety Research Institute (ESRI), Swansea University, Swansea SA1 8EN.

*Email: C.Dunnill@swansea.ac.uk

Abstract

Due to the prohibitive financial expense and logistical difficulties of a wholesale changeover from natural gas to hydrogen, hydrogen-enriched natural gas (HENG) offers a more viable intermediate solution for offsetting the carbon dioxide output of domestic gas usage and reducing the blow-out susceptibility of natural gas flames. In order to formulate a practically useful description of the blow-out threshold, the present work addresses the minimum energy per unit volume of premixed gas required for the sustained combustion of HENG fuels with molar hydrogen concentrations between zero and 50 mol%. By considering a ring burner comprising circular burner jet apertures with diameters in the range 1.0-2.4 mm, this critical energy density was demonstrated to increase linearly with the mean velocity of the admitted gas premixture, approaching a value that was common to all of the investigated HENG compositions in the limit of zero flow. Furthermore, despite flame morphology varying substantially as a function of flow conditions, the visible surface area of critically stable flames consistently exhibited an empirical squared dependence on the power generated by combusting fuel. By combining these correlations, the onset of blow-out was shown to be well-

approximated by a formula that relates the critical surface-averaged laminar burning velocity to the mean velocity of gas molecules at the burner jet. This model provides a simplified means of predicting blow-out conditions from measurable input parameters and could serve as an invaluable asset for the design of new HENG burner systems or the retrofitting of existing natural gas appliances.

Keywords: Hydrogen-enrichment; Natural gas; Flame stability; Blow-out; Laminar burning velocity; Aperture diameter.

1. Introduction

As an intermediate step towards a pure hydrogen gas network, hydrogen-enriched natural gas (HENG) offers a valuable means of reducing domestic or industrial carbon dioxide emissions without necessitating a prohibitively expensive overhaul of existing end-use appliances[1]. Indeed, whilst several governments have declared a "climate emergency" due to the emerging threats of anthropogenic climate change, none have yet implemented wholesale disruptive modifications to energy infrastructure on a national scale. The rapid, expensive international changeover from coal gas to natural gas in the 1960s-70s[2] provides a useful precedent for such changes, but, due to both the increased global population and the relative ubiquity of gas appliances, an equivalent present-day operation would incur a far greater financial cost. For this reason, hydrogen-enrichment of natural gas offers a more viable option for the partial amelioration of gas networks; HENG mixtures of up to 20 mol% hydrogen have already been utilised locally at trial sites such as Keele University in the UK[3] and the Ameland municipality of the Netherlands[4], while lower concentrations have been introduced at the utility scale through power-to-gas installations such as the Thüga plant in Frankfurt, Germany[5].

Alongside the clear environmental benefits of partially substituting natural gas for hydrogen, hydrogen-enrichment also reduces the susceptibility of laminar flames to a destabilising phenomenon known as “lifting” or “blow-off”, wherein the base of the flame becomes detached from the rim of the burner jet[6]. This effect typically occurs when the air/fuel premixture introduced to the burner is insufficiently fuel-rich, and the instability typically culminates in the eventual extinction, or “blow-out”, of the flame. Since seminal investigations into the blow-off phenomenon by authors including Lewis and von Elbe[7], von Elbe and Mentser[8], and Putnam and Jensen[9], researchers have arrived at a consensus that the blow-out threshold is intrinsically dependent on the relationship between the burning velocity of reactants at the flame front and the jet velocity of the air/fuel premixture. In particular, the jet velocity and laminar burning velocity are commonly used to estimate characteristic flow and reaction times, respectively, for a given flame system[10-14]; the ratio of these two quantities is defined as the Damköhler number, which provides a qualitative indication of whether a flame is susceptible to blow-out and serves as a foundation for building a more quantitative understanding of the conditions required to induce flame extinction.

However, the local laminar burning velocity at a given location on the flame surface is strongly influenced by flame stretch[15-21], which comprises the summed contributions of aerodynamic strain, caused by velocity deviations tangential or perpendicular to the flame front, and surface curvature. These stretching components are themselves dependent on various thermo-physical and chemical characteristics of the combusting air and fuel, such as the mass density, thermal conductivity, specific heat capacity and mass diffusion coefficient of the premixture, the activation energy and enthalpy change of the combustion reaction, and the temperature variation at the flame front[19-21]. It is therefore fundamentally difficult to formulate a general description of the blow-off onset in terms of the Damköhler number alone. Whilst thermal treatments provide an analytic basis for approximating the velocity profile of a

laminar flame system[21-32], these interpretations are often undermined by unrealistic assumptions regarding the kinetics of the underlying reaction mechanisms[33]. Consequently, modern researchers typically rely on computational techniques to simulate the reaction dynamics of a given flame system[34-45], thereby limiting the validity of their conclusions to a restricted range of fuel compositions, burner architectures and flow conditions.

In order to establish a more general relationship between jet velocity and laminar burning velocity at the onset of blow-out, the present investigation explores the instability threshold of a commercial cooktop ring burner as a function of HENG fuel composition, air-to-fuel ratio, premixture flow rate and jet aperture diameter. A core ethos of this work is that the surface-averaged characteristics of a critically stable flame should be expressed in terms of measurable experimental quantities, without resorting to numerical simulations of the velocity flow field or reaction dynamics. Moreover, the analysis has been targeted towards real-world domestic applications by ensuring that the selected system parameters are representative of typical household burner configurations[46]: the study considers interchangeable circular jets with aperture diameters in the range 1.0-2.4 mm, whilst the combustion power output was limited to values of less than 80 W per jet. For HENG fuels with hydrogen concentrations between zero and 50 mol%, novel insights into the blow-out phenomenon are provided by a semi-empirical model that relates the critical energy density of combusting reactants to the volumetric premixture flow rate, alongside correlations between the visible surface area and total power output of critically stable flames. Since the applicability of the formulation is not limited by the highly disparate thermo-physical[47] and combustion[48] properties of natural gas and hydrogen, it is reasoned that formulae derived herein are potentially adaptable to other fuel mixtures and jet configurations, providing experimentalists with an invaluable template for investigating blow-out across a plethora of burner systems.

2. Materials and Methods

2.1. Measurement of the blow-out onset

To emulate the stability behaviour of real-world natural gas appliances for different compositions of HENG fuel, the threshold of blow-out was investigated using a JP21 Phoenix ring burner (JP Burners Ltd.) equipped with twenty-one interchangeable brass burner jets; circular jet apertures were employed exclusively throughout the study, with diameters of 1.0 mm, 1.3 mm, 1.5 mm, 1.7 mm, 2.0 mm or 2.4 mm. All burner jets were drilled in-house using drill bits with a stated tolerance of 0.05 mm, which has been assumed equal to the standard uncertainty in the stated aperture diameter values. As illustrated schematically in Fig. 1, bottled G20 natural gas (identical to pure methane) and hydrogen were premixed at rates of 0-5 L min^{-1} and 0-2 L min^{-1}, respectively, with the volumetric flow rate of each gas maintained at a desired value by a designated Aalborg mass flow controller (MFC). A third Aalborg MFC was similarly used to premix the HENG fuel with up to 50 L min^{-1} of compressed air, and the resulting air/fuel premixture was introduced to the burner ring via a quarter-turn ball valve and resettable flash-back arrestor (FA). Flames were initiated at the outlet of each burner jet through use of a handheld piezoelectric igniter.

After setting the composition and flow rate of the HENG mixture, stable combustion was achieved by premixing compressed air into the fuel at a sufficiently low rate of flow. With the flow rates of hydrogen and G20 natural gas held constant, flame stability was monitored continuously upon increasing the total air flow rate stepwise in increments of 0.1 L min^{-1}, allowing approximately five seconds of observation at each step. The onset of blow-out was deemed to coincide with the first flame extinction event, and the reliability of this threshold value was improved by repeating the estimation process at least three times for each flow combination of hydrogen and G20 natural gas; in the case of an anomalous result, such as

premature flame extinction due to the presence of an air draught, further repeat cycles were conducted as required. Over the course of the investigation it was discovered that threshold air flow rate estimates within a given set of triplicate tests typically encompassed a range of up to 0.4 L min^{-1}; accordingly, the standard uncertainty in the mean flow rate has been assigned a value of 0.2 L min^{-1} in all cases. Despite gas introduction taking place at a single point on the outer circumference of the burner ring, no preferential ordering was observed in the sequence of flame extinction and all twenty-one flames were visually equivalent in size and morphology. For this reason, it has been assumed throughout the investigation that gas flow was distributed approximately equally between the burner jets.

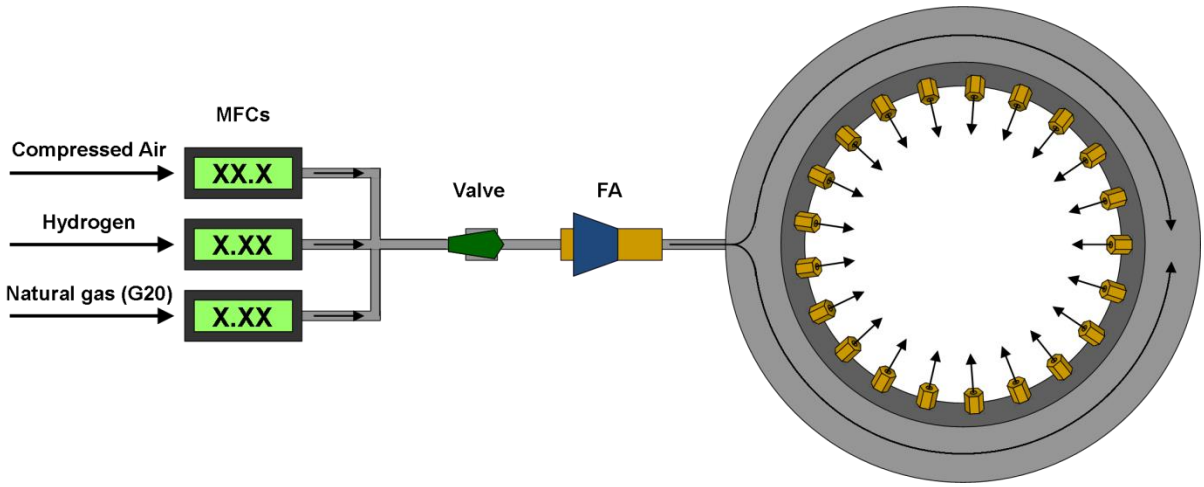

Fig. 1. Illustration of the ring burner setup employed to investigate the onset of blow-out in laminar HENG flame systems. Arrows in the diagram indicate the flow directions of compressed air, hydrogen and G20 natural gas, which were introduced to the burner ring via a resettable flash-back arrestor (FA) at rates controlled independently by designated mass flow controllers (MFCs); volumetric flow rates were displayed in units of L min^{-1} to a precision of 0.1 L min^{-1} in the case of compressed air and 0.01 L min^{-1} for both hydrogen and natural gas.

In addition to varying the aperture diameters of the burner jets, the hydrogen content of the HENG fuel was adjusted between zero and 50 mol% at intervals of 10 mol%, with nine

values of fuel flow rate investigated for every HENG composition. These values of fuel flow rate were addressed in a staggered order rather than sequentially, thereby facilitating identification of any systematic error within each dataset. Between testing of different HENG compositions, all burner jets were removed from the burner ring and cleaned by ultrasonication in dilute sulphuric acid for several minutes, before being rinsed in deionised water, dried under flow of air and remounted in the burner ring; this protocol ensured that subsequent measurements were not affected by accumulated combustion products.

2.2. Estimation of visible flame surface area and mean laminar burning velocity

Whilst investigating the instability characteristics of HENG flames associated with jet aperture diameters of 1.3 mm, 1.7 mm and 2.4 mm, an individual flame profile was photographed at the onset of blow-out for all combinations of HENG composition and fuel flow rate; it should be noted that flame imaging at this critical threshold was possible due to the time differences between extinction events at different burner jets. Photographs were recorded using an 8 megapixel iSight camera clamped at a fixed position relative to the burner ring, and the camera was set to maintain a constant focal length so that the distance between pixels was approximately invariant between consecutive images.

For each photographed flame, a MATLAB program was implemented to approximate the position and orientation of the central flame axis by locating the half-maximum cumulative intensity of the blue component within every row of image pixels. The program subsequently performed a preliminary estimate of the flame edge pixel locations with respect to this axis by maximising the function

$$g(x,y) = I(x,y)\left|\frac{\mathrm{d}I(x,y)}{\mathrm{d}x}\right| + I(-x,y)\left|\frac{\mathrm{d}I(-x,y)}{\mathrm{d}x}\right|, \quad (1)$$

where I denotes the blue component of pixel intensity at an axial coordinate distance y, which is zero at the aperture rim and increases to a value y_{tip} at the visible flame tip, and a radial

coordinate distance x, which has its origin at the flame axis. In order to obtain a more accurate representation of the visible flame surface, the variation of x at the photographed flame edge, x_{edge}, was fitted as a function of y by applying a non-linear regression protocol to the preliminary edge position estimates in conjunction with a fitting function of the form

$$x_{\mathrm{edge}} = \pm(c_2 y^2 + c_1 y + c_0)\sqrt{\ln\left(\frac{y_{\mathrm{tip}}+y_0}{y+y_0}\right)}; \tag{2}$$

here, the constants c_0, c_1 and c_2 are independent fitting variables and y_0 is a constant, positive-valued y-offset that prevents x_{edge} behaving asymptotically at the aperture rim. The overall uncertainty in x_{edge} was approximated by calculating the standard deviation of the preliminary edge position estimates from the edge function defined by Eq. (2). A typical result of the outlined fitting procedure is illustrated in Fig. 2a, which depicts the photographed profile of a critically stable HENG flame with the estimated flame axis and edge function overlaid onto the image; this particular example corresponds to a total premixture flow rate of 12.46 $\mathrm{cm^3\ s^{-1}}$ per jet, a jet aperture diameter of 1.7 mm, and a hydrogen fuel concentration of 30 mol%.

Having determined the pixel coordinates of the visible flame edge, calibration photographs were prepared to estimate the absolute radial distance to the flame edge as a function of axial distance from the aperture rim. As shown in Fig. 2b, these calibrations were conducted by first setting a Vernier calliper to a distance of 10.00 mm and positioning it normal to the jet aperture, before using ImageJ software to calculate the number of pixels, N_{scale}, between the rim and the base of the calliper body. Provided that the Vernier calliper was photographed from the same position and at the same focal length as the imaged flame profiles, the absolute axial or radial distance between pixels was calculable as the product of the corresponding coordinate distance and a scaling factor given by

$$C_{\mathrm{pix}} = \frac{10.00\ \mathrm{mm}}{N_{\mathrm{scale}}}. \tag{3}$$

In order to account for small changes in camera position during data acquisition, N_{scale} was averaged over seven calibration photographs for every value of jet aperture diameter; these photographs were recorded prior to changing the HENG composition in preparation for the next sequence of nine flame images.

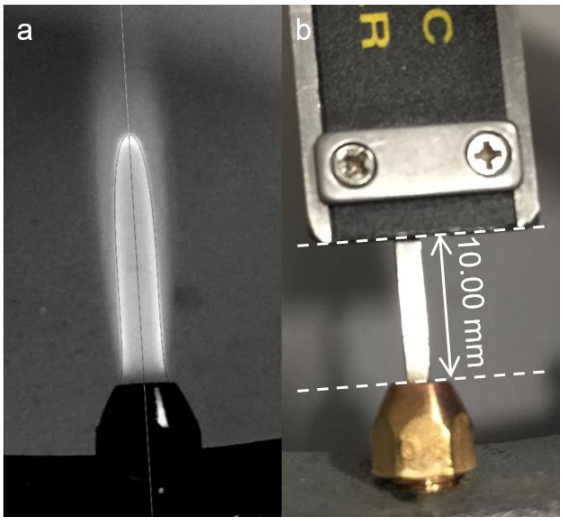

Fig. 2. Photographed HENG flame profile at the onset of blow-out (jet aperture diameter = 1.7 mm; fuel hydrogen concentration = 30 mol%; total flow rate = 12.46 cm^3 s^{-1} per jet) (a), alongside one of a group of seven calibration photographs used to determine the distances between image pixels (b). A line through the centre of the flame profile (coloured black within the region of the flame and white elsewhere) marks the estimated flame axis, whilst two axisymmetric black curves depict the edge fitting function generated using Eq. (2).

The visible flame surface area, A_{BO}, was computed from Eq. (2) via the approximation

$$A_{\mathrm{BO}} \approx \pi C_{\mathrm{pix}}^2 \sum_{i=1}^{N-1} \left(x_{\mathrm{edge,i+1}} + x_{\mathrm{edge,i}}\right) \sqrt{\left(x_{\mathrm{edge,i+1}} - x_{\mathrm{edge,i}}\right)^2 + \delta y^2}, \qquad (4)$$

which arises from subdividing an axisymmetric flame profile into N-1 trapezoidal area elements (1,000 elements were used for all flame profiles) of axial height $C_{pix}\delta y$; the surface area associated with element i corresponds to the trapezial area of its lateral face, which is

bounded by circular top and bottom faces of radii $C_{\mathrm{pix}}x_{\mathrm{edge,i+1}}$ and $C_{\mathrm{pix}}x_{\mathrm{edge,i}}$, respectively. For simplicity, area contributions from the small volume of "dead space" between the burner rim and the base of the visible flame were included in each A_{BO} estimate, even though there is insufficient energy density within this region for combustion to occur[9, 49]; however, as the volume of the dead space region was observed in all cases to be much smaller than the total volume of the visible flame, it was deemed reasonable to neglect this source of systematic error.

Following summation over all N-1 area increments, the mean laminar burning velocity with respect to the unburned air/HENG premixture, $S_{\mathrm{L,BO}}$, can be calculated by recognising that the condition

$$S_{\mathrm{L,BO}} \approx \frac{Q_{\mathrm{tot}}}{A_{\mathrm{BO}}} \tag{5}$$

must be invoked to satisfy mass conservation[17, 44, 45, 50], where Q_{tot} denotes the volumetric premixture flow rate; here it has been implicitly assumed that gas density was approximately constant throughout the flame, whilst acknowledging that $S_{\mathrm{L,BO}}$ is defined as the velocity component normal to the flame surface. It should be further noted that whilst $S_{\mathrm{L,BO}}$ represents the mean laminar burning velocity averaged over the entire visible flame front, the laminar burning velocity at a given surface location may locally deviate from $S_{\mathrm{L,BO}}$ due to aforementioned stretching effects.

2.3. Parameter fitting and estimation of uncertainties

Provided that it is possible to define a function f in terms of a set of independent variables, the associated standard error in f, σ_{f}, can be calculated using the formula

$$\sigma_{\mathrm{f}} = \left(\sum_{\mathrm{i}} \left(\frac{\partial f}{\partial a_{\mathrm{i}}} \sigma_{\mathrm{i}} \right)^2 \right)^{1/2}, \tag{6}$$

where σ_i is the estimated uncertainty in variable a_i and summation is performed over all of the independent quantities that influence f. The form of Eq. (6) is generally valid, and thus it was applied throughout the present work without further justification.

In addition to the uncertainty estimates discussed in Sections 2.1 and 2.2, a standard uncertainty of 8.3×10^{-2} cm^3 s^{-1} was assumed in the measured volumetric flow rates of both hydrogen and natural gas, consistent with a standard uncertainty of 4.0×10^{-3} cm^3 s^{-1} per jet. This estimate is based on an assumption of 95% confidence that the value measured by the relevant MFC was accurate to within the final significant figure displayed, equal to 1.7×10^{-1} cm^3 s^{-1} for both fuel gases. As reasoned in Section 2.2, the rate of primary air flow to the burner ring was assigned a standard uncertainty value of 0.2 L min^{-1}, equivalent to 1.6×10^{-1} cm^3 s^{-1} per jet. Where required, conversion between volumetric and molar quantities was achieved through application of the ideal gas law, with standard values of 25 ˚C and 1 atm assumed for the gas temperature and pressure, respectively.

The overall uncertainty in flame surface area was estimated by applying Eq. (6) in conjunction with Eq. (4); within this calculation, uncertainties in the radial flame edge coordinates, $x_{edge,i}$, were included alongside the uncertainty in the scaling factor C_{pix}. It should be noted that the uncertainty in a given $x_{edge,i}$ measurement was dependent on the edge fitting function defined by Eq. (2), which was in turn constructed from the combination of all N radial coordinates. Consequently, the $x_{edge,i}$ values were correlated through the form of the fitting function, and thus they cannot be regarded as independent variables in Eq. (6); for this reason, it was considered preferable to estimate the combined uncertainty in the N radial coordinates by calculating the product of the standard deviation in $x_{edge,i}$ and the root mean squared derivative of A_{BO} with respect to $x_{edge,i}$.

During analysis of the measured relationship between volumetric flow rate and the energy density of combusting fuel, independent linear fits associated with different HENG

compositions but identical jet aperture diameter appeared to intersect at a common energy density, U_0, at zero flow. In order to estimate the value of U_0 from a plot of energy density as a function of flow rate, the weighted mean of the y-intercept was calculated with weighting factors set equal to the reciprocal of the fitted gradients. Correspondingly, the standard uncertainty in U_0 was estimated by adopting the same weighting factors to compute the weighted standard deviation from the mean.

3. Results and Discussion

3.1. Relationship between combustion energy density and premixture flow rate

In order to model the blow-out limit of a premixed HENG flame in terms of the surface-averaged laminar burning velocity normal to the flame front, $S_{L,BO}$, and the mean velocity of reactants at the jet aperture, u_J, it is instructive to first consider how the onset of instability is related to the energy generated by complete combustion per unit volume of the gas premixture. Defining the total power production from complete combustion, P_r, as

$$P_r \equiv H n_V Q_f, \tag{7}$$

where H denotes the molar enthalpy change of the combustion reaction, Q_f is the volumetric fuel flow rate and n_V is the molar density of gas molecules at standard temperature and pressure (25 ˚C and 1 atm), the critical energy density at the blow-out threshold, U_{BO}, is given by

$$U_{BO} \equiv \left(\frac{P_r}{Q_{tot}}\right)_{BO} = H n_V \left(\frac{Q_f}{Q_{tot}}\right)_{BO}, \tag{8}$$

where Q_{tot} is the total volumetric flow rate of the premixture and the suffix "BO" signifies the condition of critical stability. It follows from Eq. (5), which relates $S_{L,BO}$ to the critical surface area of the visible flame front, A_{BO}, that

$$S_{L,BO} \approx \frac{P_r}{A_{BO} U_{BO}} = \frac{H n_V Q_f}{A_{BO} U_{BO}}, \tag{9}$$

indicating that the properties of $S_{L,BO}$ may be understood by considering how the variables A_{BO} and U_{BO} vary in terms of the fuel composition, primary air content and jet aperture dimensions. As acknowledged in the Introduction, whilst a phenomenological understanding of $S_{L,BO}$ may be formulated by using numerical simulations to model the reaction dynamics and temperature profile of a flame, discrepancies between experiment and theory typically arise from the reaction-specific nature of this approach. Instead, the present analysis is founded on a more rudimentary but general method of approximation based on the balance of energies at the flame front.

As the travelling premixture approaches the combusting fuel downstream, it eventually heats to a temperature that is sufficient for reaction to commence. The region of space in which it is possible for combustion to take place is defined as the "reaction zone", whilst approaching air and fuel that has yet to overcome the reaction barrier occupies a "preheat zone" at the core of the flame. If one assumes that from a total energy U generated per unit volume of combusting premixture, an amount U_{heat} is imparted to incoming reactants and the remainder, U_0, is released to the system surroundings, energy conservation demands that

$$U = U_{\mathrm{heat}} + U_0. \tag{10}$$

In order for combustion to be sustained, the energy per unit volume transferred to incident reactants must exceed the total energy density needed to overcome the reaction barrier, E_A, and from this consideration it follows that the minimum power required for continuous reaction is equal to the product of E_A and Q_{tot}. Defining ω_r as the overall volumetric rate of premixture combustion in the reaction zone, it is therefore necessary that a stable flame obeys the condition

$$(U - U_0)\omega_{\mathrm{r}} \geq E_{\mathrm{A}} Q_{\mathrm{tot}}, \tag{11}$$

where it should be recognised that no assumptions have been made regarding the functional dependences of ω_r or E_A. Hence, the onset of blow-out can be described by an expression of the form

$$U_{BO} = \xi_r Q_{tot} + U_0, \quad (12)$$

where E_A and ω_r have been combined to generate a new reaction parameter, ξ_r. For the purposes of the present investigation, the occurrence of flame flash-back[51] is to be ignored; flame stability is practically infeasible at very low values of Q_{tot} as a consequence of this phenomenon, which is characterised by the flame front propagating backwards into the preheat zone of the unreacted premixture.

The validity of Eq. (12) was investigated by measuring U_{BO} as a function of Q_{tot} for HENG fuels of molar hydrogen fraction, X_{H2}, between zero and 0.5 and burner jets with aperture diameters, D_J, in the range 1.0-2.4 mm; these data are presented in Fig. 3. The H estimates used to calculate U_{BO} have been computed from tabulated lower heating values (LHVs) of methane, H_{CH4}, and hydrogen, H_{H2}, through application of the compositionally weighted formula

$$H = (1 - X_{H2})H_{CH4} + X_{H2}H_{H2}, \quad (13)$$

where standard LHVs of 802.54 kJ mol^{-1} and 241.85 kJ mol^{-1} have been assigned to H_{CH4} and H_{H2}, respectively[52]. One should note that the LHV of a combusting gas is defined as the enthalpy change under standard initial conditions (25 ˚C and 1 atm) assuming that all products remain in the gaseous state; this measure is deemed appropriate in the present circumstances, as the water product was released as vapour into the surroundings. It is evident from Fig. 3 that U_{BO} exhibited a linear dependence on Q_{tot} over the measured parameter space of D_J and X_{H2} values, in turn indicating that either a direct proportionality existed between E_A and ω_r or that both of these variables were approximately independent of Q_{tot}. Linear fits applied at constant

D_J are shown to intersect at a common value of U_0, which suggests that the energy per unit volume of combusting premixture released to the flame surroundings was not significantly influenced by the value of X_{H2}. However, since Eq. (8) imposes the condition that U_{BO} cannot exceed the product Hn_V, the linear trends in Fig. 3 must become physically invalid above a particular value of Q_{tot}. There is similarly no justification for extending the observed trends below the experimental Q_{tot} range, and one cannot reasonably assume that the observed constancy of ξ_r persists in the limit of zero flow. For these reasons, caution should be applied when extrapolating the fitted relationships beyond the scope of the present measurements.

The invariance of U_0 for a given configuration of burner jets is an intriguing result, as it indicates that all dependence of U_{BO} on the particular reaction or flow characteristics of the HENG fuel are comprised within the gradient function, ξ_r. Moreover, further examination of Fig. 3 reveals an approximate inverse proportionality between U_0 and D_J: as shown in Fig. 4, the measured relationship between U_0 and the reciprocal of D_J is well-characterised by a linear trend that passes through the origin of the plot, exhibiting a coefficient of determination, R^2, of 0.97. From this result one may infer that the product U_0D_J is not significantly influenced by X_{H2} or D_J, and thus it may be regarded as a universal property of the burner system. It is nevertheless important to recognise that since the present investigation solely addresses the stability of flames anchored above brass jets with circular apertures, the empirical results presented in Figs. 3 and 4 cannot be applied directly to alternative jet types. Indeed, research has shown that modification of the aperture shape can significantly affect the morphology and stability thresholds of a laminar flame[53, 54].

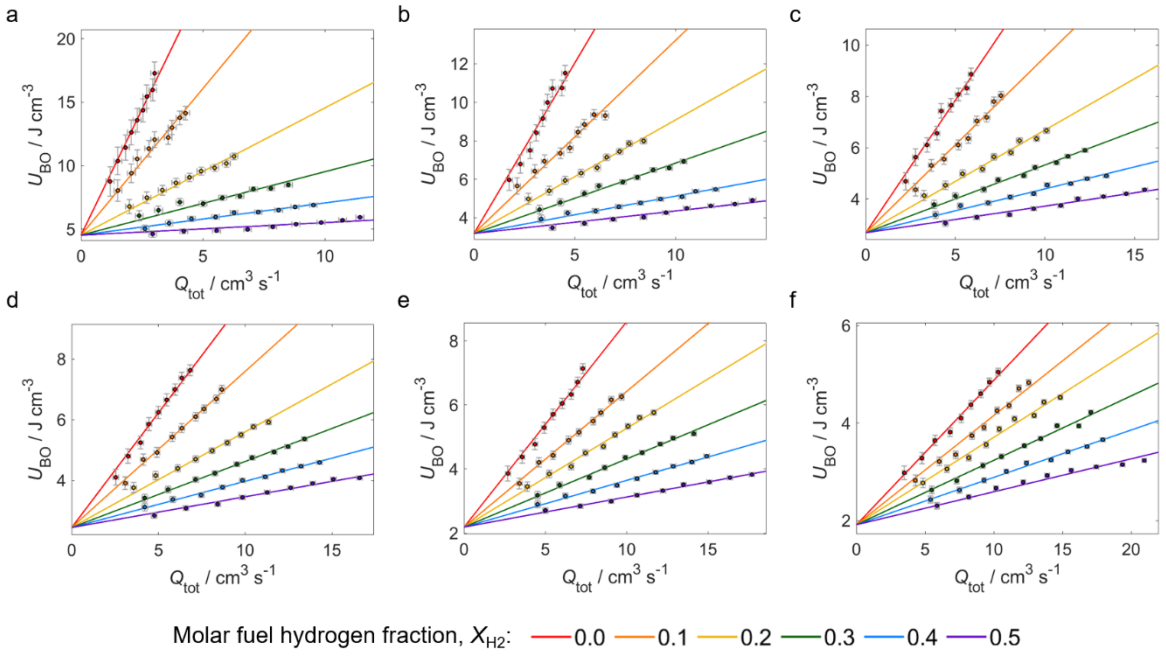

335

336 Fig. 3. Measured relationships between the combustion energy density at the onset of blow-
337 out, U_{BO}, and the total volumetric premixture flow rate per jet, Q_{tot}, for molar fuel hydrogen
338 fractions, X_{H2}, between zero and 0.5; the plotted data-sets correspond to jet aperture diameters
339 of 1.0 mm (a), 1.3 mm (b), 1.5 mm (c), 1.7 mm (d), 2.0 mm (e) and 2.4 mm (f), and linear fits
340 have been constructed in accordance with Eq. (12).

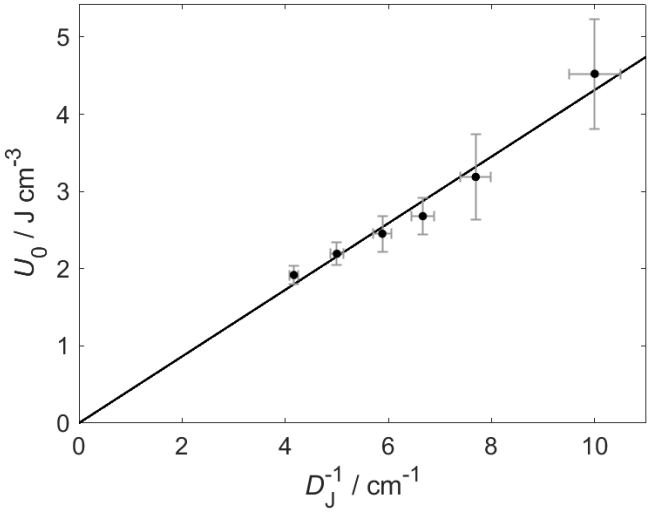

341

Fig. 4. Variation of U_0, the y-intercept of the $U_{BO}(Q_{tot})$ fits depicted in Fig. 3, as an inverse function of the jet aperture diameter, D_J; the form of this relationship is approximated by a linear fit that intersects the origin the plot.

To illustrate how the onset of blow-out varies for different premixed gas flows, researchers commonly evaluate the primary air fraction at this threshold[55-57], λ_{BO}, by combining the measured molar air flow rate, Q_a, the molar flow rate of fuel, Q_f, and the stoichiometric molar ratio of air to fuel, n_{st} according to the definition

$$\lambda_{BO} \equiv \frac{1}{n_{st}}\left(\frac{Q_a}{Q_f}\right)_{BO}, \tag{14}$$

which equals unity in the special case of a stoichiometric air/fuel premixture. Combining Eq. (8) and Eq. (12) to eliminate U_{BO} generates the quadratic equation

$$\xi_r {Q_{tot}}^2 + U_0 Q_{tot} - P_r = 0 \tag{15}$$

with the physical solution

$$Q_{tot} = \frac{U_0}{2\xi_r}\left(\sqrt{1 + 4\frac{\xi_r P_r}{{U_0}^2}} - 1\right), \tag{16}$$

whereupon Eq. (14) may be used to show that

$$\lambda_{BO} = \frac{U_0 H n_V}{2 n_{st} \xi_r P_r}\left(\sqrt{1 + 4\frac{\xi_r P_r}{U_0^2}} - 2\frac{\xi_r P_r}{U_0 H n_V} - 1\right); \tag{17}$$

in order to derive Eq. (17) from Eq. (16) one must first note that Q_{tot} is by definition equal to the sum of Q_f and Q_a. In contrast to Eq. (14), which expresses λ_{BO} in terms of two variable flow rates, the inclusion of U_0 and ξ_r in Eq. (17) reduces the dependence of λ_{BO} at given D_J and X_{H2} to a single variable quantity, P_r.

The efficacy of the present treatment is further explored in Fig. 5, which depicts the variation of λ_{BO} as a function of P_r for multiple combinations of D_J and X_{H2}. The fitting functions supplied by Eq. (17) provide a satisfactory representation of the plotted experimental

trends, and they are closely consistent with comparable $\lambda_{BO}(P_r)$ relationships derived previously by the present authors from a meta-analysis of published empirical models[46]. A remarkable feature of the plotted data-sets is the near-convergence of $\lambda_{BO}(P_r)$ at constant D_J in the limit of zero flow, which may be quantitatively understood by considering the behaviour of Eq. (17) within this regime. In particular, as P_r goes to zero and Eq. (17) becomes

$$\lim_{P_r \to 0} \lambda_{BO} = \frac{1}{n_{st}} \left(\frac{H n_V}{U_0} - 1 \right), \tag{18}$$

the effect of changing n_{H2} is almost negated by a counteractive variation in H. However, it is once again important to recognise that since the form of Eq. (12) has not been verified for this limiting case, Eq. (17) is not necessarily reliable below the experimental range of P_r values.

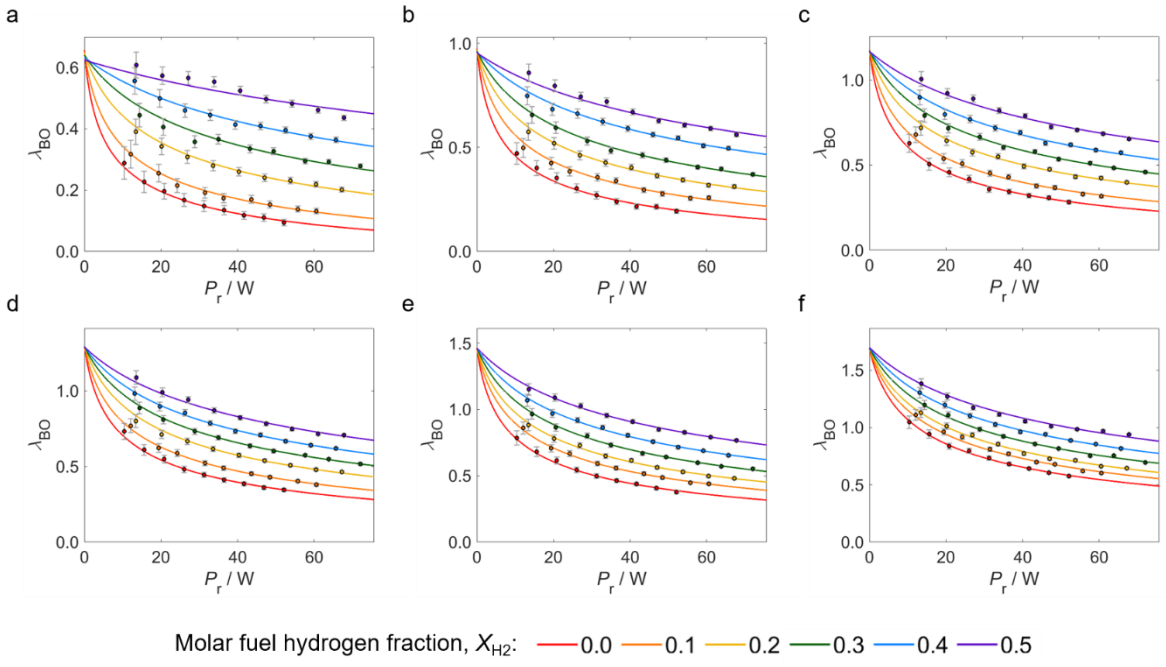

Fig. 5. Experimental and fitted variations of the critical primary air fraction, λ_{BO}, with respect to the power generated from complete fuel combustion, P_r, for jet aperture diameters of 1.0 mm (a), 1.3 mm (b), 1.5 mm (c), 1.7 mm (d), 2.0 mm (e) and 2.4 mm (f) and molar fuel hydrogen fractions, X_{H2}, between zero and 0.5.

3.2. Surface-averaged laminar burning velocity at the onset of blow-out

Based on the form of Eq. (9), the functional dependences of $S_{L,BO}$ on the parameters of a flame system can be derived by combining the results of Section 3.1 with knowledge of the relationship between P_r and A_{BO}. To facilitate this analysis, A_{BO} estimates were obtained from the fitted surfaces of 162 flame profiles encompassing various combinations of D_J, X_{H2} and Q_f; all of these images are provided in Figs S1, S2 and S3 of the Supporting Information, corresponding to D_J values of 1.3 mm, 1.7 mm and 2.4 mm, respectively, and, for ease of reference, a sample of photographs from Fig. S2 is reproduced in Fig. 6. From the pictured profiles it is evident that the flames deviated from the straight-sided form of an ideal Bunsen flame, and that the magnitude of this divergence was enhanced by reducing the hydrogen content of the HENG fuel or by increasing the total volumetric flow rate of the premixture. For this reason, it is fundamentally difficult in the present case to approximate the form of the velocity flow field from a simplified description of the flame morphology[18]; instead, all formulations presented in this section are justified through empirical relationships between $S_{L,BO}$ and measurable system variables. Whilst qualitative arguments are proffered when discussing the physical origin of experimental correlations, the development of more rigorous phenomenological explanations are left to future studies.

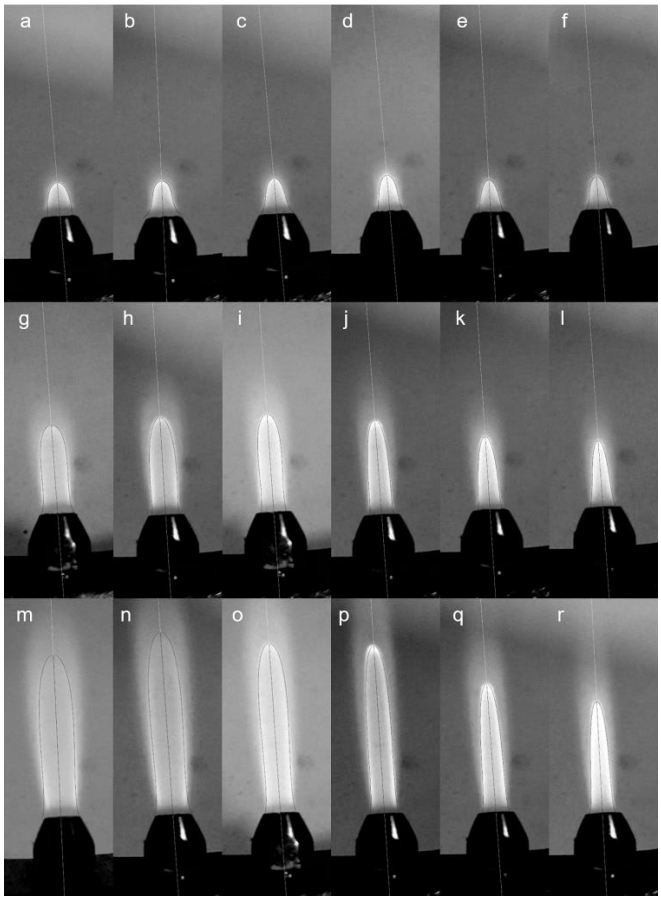

Fig. 6. Surface-fitted HENG flame profiles anchored above a brass jet of 1.7 mm aperture diameter, photographed at the onset of blow-out; these images correspond to images 1-6 (a-f), 25-30 (g-l) and 49-54 (m-r) in Fig. S2 of the Supporting Information, with the total premixture flow rate, Q_{tot}, increasing down the figure (all values of Q_{tot} and the constituent flow rates are detailed in Table S1 of the Supporting Information). The fuel hydrogen fraction, X_{H2}, was set to a value of zero (a, g and m), 0.1 (b, h and n), 0.2 (c, i and o), 0.3 (d, j and p), 0.4 (e, k and q) or 0.5 (f, l and r). The central axis of each profile is marked by a line coloured black inside the flame region and white elsewhere.

In Fig. 7, the measured variation of A_{BO} is plotted as a function of P_r for all combinations of X_{H2} and D_J; in each case, the observed correlation is well-described by the empirical equation

$$\sqrt{A_{BO}} = \frac{1}{p'} P_r + L_0, \quad (19)$$

where L_0 and p' are X_{H2}- and D_J-dependent constants with units of distance and power per unit distance, respectively. Whilst the physical origin of this relationship between P_r and A_{BO} is unclear, it is qualitatively instructive to recognise that the quotient P_r/A_{BO}, which is equivalent to the mean magnitude of power flux, J_r, required for stable combustion, diminished as the size of the flame was increased. A possible rationale for this effect is that an enlarged flame affords a greater average distance between the jet aperture and the flame front, thereby suppressing the rate of heat extraction by the thermally conductive burner jet[49].

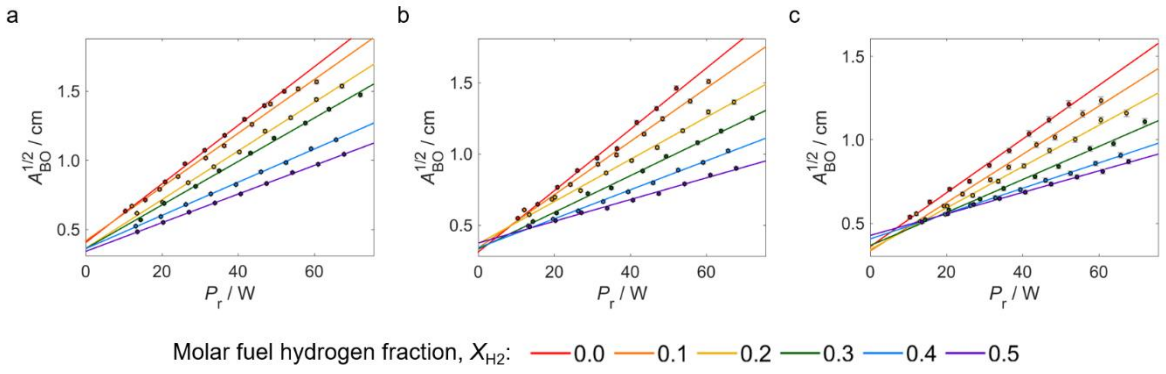

Fig. 7. Linearly fitted experimental relationships between the square root of visible flame surface area at the blow-out threshold, A_{BO}, and the total power released from complete fuel combustion, P_r, for jet aperture diameters of 1.3 mm (a), 1.7 mm (b) and 2.4 mm (c) and molar fuel hydrogen fractions, X_{H2}, between zero and 0.5.

Despite the A_{BO} and P_r measurements adhering closely to the correlation predicted by Eq. (19), it is important to emphasise that this empirical description is not necessarily consistent with physical first principles. Indeed, a particularly problematic feature of Eq. (19) is that P_r becomes negative when A_{BO} is less than the square of L_0, which implies that flames below this size threshold are stable for all positive values of P_r and hence immune to blow-out. To illustrate the implausibility of this result, Fig. 8 shows the variation of J_r with respect to A_{BO}; the solid-line fits to each dataset have been generated from the expression

$$J_{\mathrm{r}} \equiv \frac{P_{\mathrm{r}}}{A_{\mathrm{BO}}} = p'\left(\frac{1}{\sqrt{A_{\mathrm{BO}}}} - \frac{L_0}{A_{\mathrm{BO}}}\right), \tag{20}$$

which is obtained directly from combining Eq. (19) with the definition of J_{r}. Although the form of Eq. (20) yields an adequate approximation of the J_{r} threshold over the experimental range of A_{BO} estimates, extrapolation to lower values implicitly assumes that the temperature profile of a sufficiently small flame can be sustained even if there is zero power density at the flame surface. Eqs. (19) and (20) therefore contravene energy conservation requirements when A_{BO} is less than or equal to the square of L_0, and thus it follows trivially that any other functional relationship between P_{r} and A_{BO} must be deemed unphysical unless P_{r} is greater than zero for all positive values of A_{BO}.

In order to improve upon Eq. (19) whilst maintaining the observed linearity of the plotted relationships in Fig. 7, one may introduce exponential correction factors into Eq. (20) to generate an alternative fitting function,

$$J_{\mathrm{r}} = p'\left(\frac{1-\exp\left(-\gamma_1 A_{\mathrm{BO}}^{n}\right)}{\sqrt{A_{\mathrm{BO}}}} - \frac{L_0\left(1-\exp\left(-\gamma_2 A_{\mathrm{BO}}^{n+\frac{1}{2}}\right)\right)}{A_{\mathrm{BO}}}\right), \tag{21}$$

where γ_1, γ_2 and n are constants. From Eq. (21) it can be shown that J_{r} vanishes at zero A_{BO} provided that n is greater than a half, while the condition

$$\gamma_1 > \gamma_2 L_0 \tag{22}$$

is imposed by the physical requirement that J_{r} is never negative for positive values of A_{BO}. The dashed lines in Fig. 8 correspond to fitting curves constructed using Eq. (21), with the constant n arbitrarily assigned a value of 1.5 in all cases.

Within the limits of the data displayed in Fig. 8, it is evident that the descriptions provided by Eqs. (20) and (21) offer a similar quality-of-fit despite differing markedly at lower values of A_{BO} due to the asymptotic behaviour of Eq. (20). The expected convergence of the

two fitting equations typically occurs within the experimental range of the measurements, although it should be noted that the discrepancy between each pair of solid and dashed curves is strongly dependent on the magnitude of n, with greater consistency between corresponding fits achieved by increasing the value of this parameter. However, since the restricted range of the present data prohibits meaningful estimation of n, one cannot reasonably use Eq. (21) to approximate the form of the $J_r(A_{BO})$ relationship as A_{BO} approaches zero; this limitation means that Eq. (21) presently offers no greater predictive power than Eq. (20), despite comprising three additional fitting parameters. Consequently, Eq. (20) is henceforth adopted as the preferable model for the $J_r(A_{BO})$ relationship, albeit with the important caveat that its form is not physically justifiable in the limit of zero surface area.

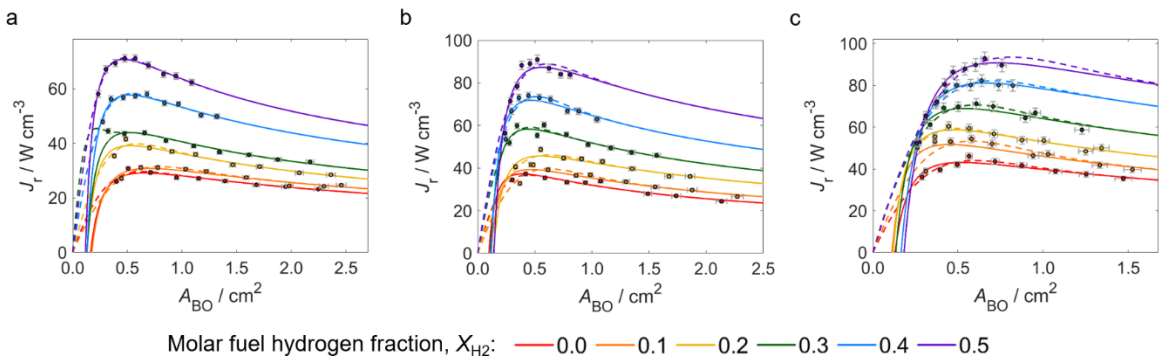

Fig. 8. Experimental variation of the surface-averaged power flux, J_r, with respect to the total surface area of the visible flame at the onset of blow-out, A_{BO}, for jet aperture diameters of 1.3 mm (a), 1.7 mm (b) and 2.4 mm (c) and molar fuel hydrogen fractions, X_{H2}, between zero and 0.5. Alternative fitting functions are provided by Eq. (20) and Eq. (21), depicted as solid and dashed lines, respectively.

By combining Eq. (19) with previous formulae, it is possible to derive an empirical relationship between $S_{L,BO}$ and the mean jet velocity of premixture molecules, u_J: using Eq. (8)

to eliminate P_r from Eq. (19), substituting for U_{BO} by recalling Eq. (12), inserting the resulting expression for A_{BO} into Eq. (5), and finally invoking the trivial relation

$$Q_{tot} = A_J u_J, \tag{23}$$

where A_J is the cross-sectional area of the jet aperture, one arrives at the approximation

$$S_{L,BO} \approx \frac{p'^2 A_J u_J}{\left(\xi_r A_J^2 u_J^2 + U_0 A_J u_J + p' L_0\right)^2}, \tag{24}$$

which incorporates all of the fitting variables from Eqs. (12) and (19). A notable characteristic of Eq. (24) is that it exhibits no explicit dependence on the shape or curvature of the flame surface, as all four fitting parameters are approximately invariant with respect to u_J despite the marked morphological differences between the flame profiles pictured in Fig. 6 and Figs. S1, S2 and S3 of the Supporting Information. Remarkably, this result implies that whilst local burning velocity is dependent on the variation of flame stretch as a function of flame surface position, the structural dependence of $S_{L,BO}$ is defined exclusively by the straightforward $P_r(A_{BO})$ description provided by Eq. (19).

In Fig. 9, $S_{L,BO}$ estimates obtained through application of Eq. (5) are plotted against the corresponding values of u_J for all combinations of D_J and X_{H2}, while fitting curves have been produced in each instance by inserting the relevant values of ξ_r, U_0, p' and L_0 into Eq. (24). All of the measured $S_{L,BO}(u_J)$ trends are characterised by an asymmetric peak function that is well-described by the empirical fits, with the only significant anomalies occurring towards the lower limit of the measured u_J range. These discrepancies may be rationalised by recalling that as a consequence of the unphysical asymptotic behaviour of Eq. (20) in the limit of zero flow, Eq. (19) deviates substantially from the true $A_{BO}(P_r)$ relationship as P_r approaches zero. Nevertheless, the form of Eq. (24) ensures that $S_{L,BO}$ vanishes at zero flow, thereby satisfying

the continuity requirement that mass is conserved between the jet aperture and the flame surface.

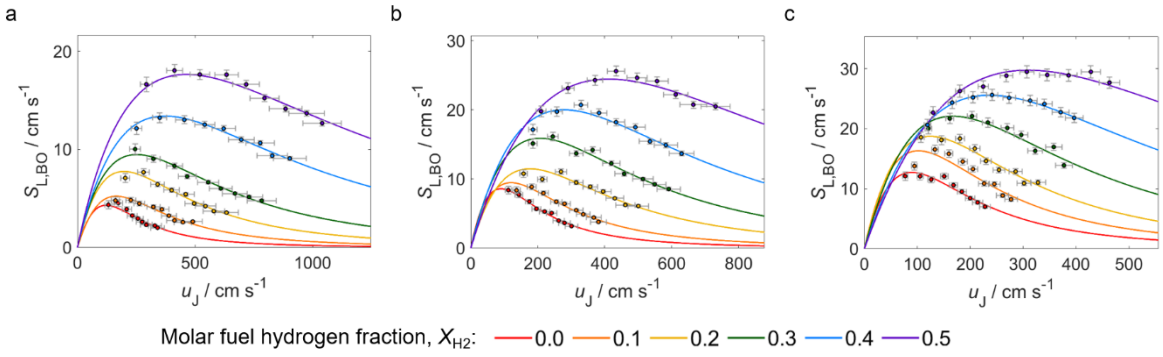

Fig. 9. Fitted variations of the surface-averaged laminar burning velocity at the blow-out threshold, $S_{L,BO}$, as a function of the mean premixture jet velocity, u_J; the plotted data correspond to jet aperture diameters of 1.3 mm (a), 1.7 mm (b) and 2.4 mm (c), with the molar fuel hydrogen fraction X_{H2} set to values between zero and 0.5.

As a final consideration, Fig. 10 addresses the variation of $S_{L,BO}$ with respect to the equivalence ratio at the blow-out threshold, ϕ_{BO}, which is by definition equal to the reciprocal of the primary air function, λ_{BO}. Fits were constructed for the plotted data-sets by formulating $S_{L,BO}(\phi_{BO})$ relationships that are consistent with the corresponding $\lambda_{BO}(P_r)$ and $S_{L,BO}(u_J)$ trends depicted in Figs. 5 and 9, respectively. This task was achieved by first combining the definitions of P_r, λ_{BO} and Q_{tot}, given respectively by Eqs. (7), (14) and (23), to show that

$$P_r = Hn_V \frac{A_J u_J}{n_{st}\lambda_{BO}+1}, \tag{25}$$

whilst rearrangement of Eq. (17) yields the expression

$$P_r = Hn_V \frac{Hn_V - U_0(n_{st}\lambda_{BO}+1)}{\xi_r(n_{st}\lambda_{BO}+1)^2}. \tag{26}$$

By equating Eqs. (25) and (26) and replacing λ_{BO} with the reciprocal of ϕ_{BO}, one obtains

$$A_J u_J = \frac{(Hn_V - U_0)\phi_{BO} - U_0 n_{st}}{\xi_r(\phi_{BO}+n_{st})}, \tag{27}$$

whereupon $S_{L,BO}$ may be expressed in terms of ϕ_{BO} by substituting for the product $A_J u_J$ in Eq. (24). Through inspection of Fig. 10, it is evident that the fitting functions generated from Eqs. (24) and (27) consistently provide a close approximation of the measured correlations between $S_{L,BO}$ and ϕ_{BO}.

A shared feature of the $S_{L,BO}(\phi_{BO})$ relationships is that the value of ϕ_{BO} at maximum $S_{L,BO}$ is close to unity, which accords with literature measurements of the unstretched laminar burning velocity, $S_{L,u}$, of HENG flames with respect to the equivalence ratio, ϕ, of the premixture[38-43, 50, 58]. However, the aforementioned effects of velocity-induced strain and flame curvature had a marked influence on the $S_{L,BO}$ estimates plotted in Fig. 10; one should recall that these stretching phenomena are visually apparent from the flame profiles pictured in Fig. 6 and Figs. S1, S2 and S3 of the Supporting Information, which progressively diverged from the straight-sided morphology of an ideal Bunsen flame with increasing jet velocity. Indeed, there are significant differences between the plotted $S_{L,BO}(\phi_{BO})$ trends and $S_{L,u}(\phi)$ relationships from the cited literature; for example, whilst a comparison of these studies reveals that $S_{L,u}(\phi)$ is approximately independent of D_J for a given HENG fuel, aperture enlargement within the present experiments caused all of the $S_{L,BO}$ maxima to increase in magnitude and shift towards lower values of ϕ_{BO}. Furthermore, the peak values of $S_{L,BO}$ are lower than corresponding estimates for an unstretched flame; in the case of methane, for instance, $S_{L,u}$ has been shown to exhibit a characteristic maximum in the range 35-40 cm s^{-1}, whereas $S_{L,BO}$ did not exceed 13 cm s^{-1} for any of the methane flames investigated herein.

It is worth noting that in the case of a slot burner setup, the presence of flame stretch makes it impossible to measure $S_{L,u}$ directly. Instead, the limiting case of zero stretch is typically approximated from the measured laminar burning velocities of stretched flames by formulating appropriate correction factors[15, 21]; to this end it is necessary to formally evaluate the local stretch rate as a function of frontal position by computing the constituent

strain and curvature components, which in turn requires a numerical treatment to determine the form of the surface velocity profile. As detailed previously, however, such considerations are beyond the specified scope of the present analysis, which is aimed exclusively at relating the surface-averaged properties of critically-stable flames to measurable system conditions.

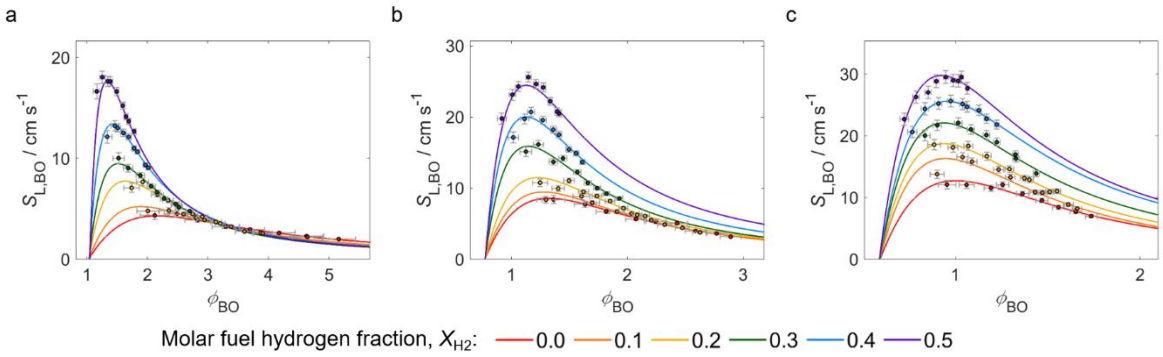

Fig. 10. Fitted experimental relationships between the mean laminar burning velocity at the blow-out threshold, $S_{L,BO}$, and the premixture equivalence ratio, ϕ_{BO}, for jet aperture diameters of 1.3 mm (a), 1.7 mm (b) and 2.4 mm (c), and molar fuel hydrogen fractions, X_{H2}, between zero and 0.5.

4. Conclusions

By circumventing the problematic and often unrealistic assumptions employed in previous phenomenological treatments of the blow-out phenomenon, the model developed herein provides a useful and experimentally justified basis for predicting the onset of instability in laminar HENG flame systems. The formulation offers novel insights into the causative factors of flame extinction in the case of premixed HENG fuels admitted to a ring burner with circular jet apertures, elucidating the relationship between the blow-out threshold and the energy density of combusting reactants. In particular, for aperture diameters in the range 1.0-2.4 mm, molar fuel hydrogen fractions between zero and 0.5, and energy flow rates of up to 80 W per jet, it has been demonstrated experimentally that:

- the critical energy density of the air/fuel premixture, which corresponds to the minimum energy per unit volume required for sustainable combustion, varies linearly as a function of the total molar flow rate;
- in the limit of zero total flow, the energy generated per unit volume of premixture at the onset of blow-out is independent of the fuel composition and exhibits an approximate inverse proportionality with respect to the jet aperture diameter;
- over the measured experimental range, the square root of the visible flame surface area varies in direct proportion to a change in the output power of combusting fuel;
- and the mean laminar burning velocity of reactants scales linearly as a function of the mean jet velocity under low-flow conditions but diminishes with increasing jet velocity in the case of fast-flowing premixtures.

Based on these results it has been shown that the surface-averaged laminar burning velocity can be expressed in terms of the mean gas jet velocity and the cross-sectional area of the jet aperture via a straightforward relationship characterised by four independent empirical fitting parameters. The derived formula is closely consistent with the measured correlation between mean gas velocities at the burner jet and the flame front, and, despite surface stretch acting to suppress the magnitude of laminar burning velocity, the model successfully reproduces the shape of the well-documented variation of unstretched laminar burning velocity with respect to the equivalence ratio of an air/HENG premixture.

Whilst the present investigation specifically addresses the blow-out characteristics of laminar HENG flames, the outlined formulation provides a consistent description of the stability threshold for a range of fuel compositions despite the notably disparate thermo-physical properties (including characteristics such as mass density, viscosity, thermal conductivity and specific heat capacity)[47] and oxidation pathways[48] of the constituent gases. For this reason, it is argued that the outlined methodology is not inherently constrained

by the nature of the fuel employed, and that the resulting theory may be readily tailored to suit alternative air/fuel premixtures. This versatility is a consequence of the eschewal of complex factors such as the temperature profile of the flame, which typically encumber existing theories; instead, the simplified approach presented herein depends only on known fuel parameters and measurable quantities that are approximately independent of jet velocity. By approximating blow-out behaviour in this way, the model provides an invaluable predictive tool for researchers throughout the field of combustion dynamics.

One caveat of the present approach is that since a single ring burner was used during the investigations, one cannot necessarily apply the same relationships to other burner architectures. Nevertheless, there remains significant scope for the analysis to be adapted to such configurations, whilst there are also opportunities to explore the phenomenological processes responsible for key results such as the relationship between the visible surface area of a critically stable flame and the power generated by combusting fuel. It would be instructive, for instance, to address how jet dimensions, fuel composition and flow conditions influence the distribution of local instabilities across the flame front, and to examine the fundamental roles of positionally variable factors such as flame stretch within the surface-averaged model. To this end, the formative insights offered by the present study provide a useful foundation for future theoretical treatments of the blow-out phenomenon.

Nomenclature

Symbols

A_{BO} Measured surface area of a visible flame profile pictured at the onset of blow-out; this threshold is defined as the first observed instance of flame extinction.

BO Suffix used to denote the threshold of blow-out.

599 C_{pix} Conversion factor defining the distance between pixels measured along the flame axis
600 in a photographed flame profile.

601 D_J Diameter of the circular jet aperture.

602 E_A Activation energy of fuel combustion per unit volume of the gas premixture.

603 g Function defined by the product of pixel intensity, I, and the derivative of intensity with
604 respect to radial distance x from the flame axis; this quantity is used to estimate the
605 location of the flame front in a photographed flame profile.

606 H Molar lower heating value of HENG combustion at standard temperature and pressure,
607 estimated by computing the compositionally weighted mean of tabulated standard
608 molar lower heating values for hydrogen and methane.

609 H_{CH4} Molar lower heating value of methane combustion at standard temperature and
610 pressure.

611 H_{H2} Molar lower heating value of hydrogen combustion at standard temperature and
612 pressure.

613 I Blue component of pixel intensity within a photographed flame profile.

614 J_r Mean magnitude of power flux at the visible surface of a critically stable flame, defined
615 as the quotient of the total power generated by fuel combustion, P_r, and the critical
616 flame surface area, A_{BO}.

617 L_0 Fitting parameter given by the y-intercept from a plot of the square root of critical flame
618 surface area, A_{BO}, versus the total power generation from fuel combustion, P_r.

619 n_{st} Molar ratio of air to fuel in a stoichiometric premixture.

620 n_V Molar volumetric density of gas molecules at standard temperature and pressure.

621 N_{scale} Estimated number of pixels in a calibration photograph between the rim of a jet aperture
622 and the base of a Vernier calliper set to a distance of 10.00 mm and positioned normal
623 to the jet aperture.

624 p' Fitting parameter given by the reciprocal of the gradient from a plot of the square root
625 of critical flame surface area, A_{BO}, versus the total power generation from fuel
626 combustion, P_r.

627 P_r Total power generated by the complete combustion of fuel molecules.

628 Q_a Measured volumetric primary air flow rate per burner jet.

629 Q_f Measured volumetric fuel flow rate per burner jet.

630 Q_{tot} Total volumetric gas flow rate per burner jet, given by the sum of the primary air flow
631 rate, Q_a, and fuel flow rate, Q_f.

632 $S_{L,u}$ Laminar burning velocity of an unstretched flame.

633 $S_{L,BO}$ Mean laminar burning velocity at the threshold of blow-out, averaged over the entire
634 surface of the visible flame.

635 u_J Mean velocity of gas molecules at the aperture of the burner jet.

636 U Volumetric energy density of the combusting premixture, assuming complete reaction
637 of the HENG fuel.

638 U_{BO} Volumetric energy density of the combusting premixture at the onset of blow-out,
639 assuming complete reaction of the HENG fuel.

640 U_{heat} Energy per unit volume transferred from combusting premixture to unreacted primary
641 air and fuel molecules entering the reaction zone.

642 U_0 Extrapolated value of U_{BO} in the limit of zero total flow; it is surmised that this quantity
643 corresponds to the heat released to the surroundings per unit volume of combusting
644 premixture.

645 x Coordinate pixel distance in the radial direction from the central axis of a photographed
646 flame profile.

647 x_{edge} Estimated radial pixel distance of the visible flame edge from the central axis of a
648 photographed flame profile.

649 X_{H2} Fractional molar concentration of hydrogen in the HENG fuel, alternatively referred to
650 as the fuel hydrogen fraction.

651 y Coordinate pixel distance parallel to the axis of a photographed flame profile, measured
652 from the rim of the burner jet aperture.

653 y_{tip} Coordinate pixel location of the visible flame tip along the axis of a photographed flame
654 profile, measured from the rim of the burner jet aperture.

655 δy Infinitesimal interval of y used to define the thickness of a circular cross-sectional disk
656 within a photographed flame profile.

657 λ_{BO} Primary air fraction at the onset of blow-out, defined as the measured molar ratio of
658 primary air to fuel divided by the stoichiometric molar air/fuel ratio, n_{st}.

659 ξ_r Gradient of the relationship between the critical volumetric energy density, U_{BO}, and
660 the volumetric premixture flow rate, Q_{tot}.

661 σ_f Estimated standard uncertainty in a variable f.

662 ϕ Equivalence ratio of the air/fuel premixture, defined as the product of n_{st} and the ratio
663 of the volumetric fuel and primary air flow rates.

664 ϕ_{BO} Equivalence ratio of the air/fuel premixture at the onset of blow-out; ϕ_{BO} is identical to
665 the reciprocal of the primary air fraction at the blow-out threshold, λ_{BO}.

666 ω_r Volumetric rate of premixture combustion.

667 Author contributions

668 Daniel Raymond Jones: Conceptualisation, Methodology, Software, Validation, Formal
669 analysis, Investigation, Data curation, Writing – Original draft preparation, Visualisation,
670 Project administration; Charles William Dunnill: Supervision, Funding acquisition.

671 Acknowledgements

672 Financial support was provided by the Welsh Government Sêr Cymru Programme and the
673 Flexis project, which is part-funded by the European Regional Development Fund (ERDF)
674 through the Welsh Government.

675 Competing interests

676 The authors declare no competing interests.

677 References

678 [1] I.A. Gondal, Hydrogen integration in power-to-gas networks, Int. J. Hydrogen Energ. 44
679 (2019) 1803-1815.
680 [2] S. Arapostathis, S. Laczay, P.J.G. Pearson, Steering the 'C-Day': Insights from the rapid,
681 planned transition of the UK's natural gas conversion programme, Environ. Innov. Soc. Tr. 32
682 (2019) 122-139.

683 [3] C.J. Quarton, S. Samsatli, Power-to-gas for injection into the gas grid: What can we learn
684 from real-life projects, economic assessments and systems modelling?, Renew. Sust. Energ.
685 Rev. 98 (2018) 302-316.
686 [4] P.E. Dodds, W. McDowall, The future of the UK gas network, Energ. Policy 60 (2013)
687 305-316.
688 [5] R. Judd, D. Pinchbeck, Hydrogen admixture to the natural gas grid, Comp. Hydrogen
689 Energy 4 (2016) 165-192.
690 [6] K.S. Kedia, A.F. Ghoniem, Mechanisms of stabilization and blowoff of a premixed flame
691 downstream of a heat-conducting perforated plate, Combust. Flame 159 (2012) 1055-1069.
692 [7] B. Lewis, G. von Elbe, Stability and Structure of Burner Flames, J. Chem. Phys. 11 (1943)
693 75-97.
694 [8] G. von Elbe, M. Mentser, Further Studies of the Structure and Stability of Burner Flames,
695 J. Chem. Phys. 13 (1945) 89-100.
696 [9] A.A. Putnam, R.A. Jensen, Application of dimensionless numbers to flash-back and other
697 combustion phenomena, Symp. on Combustion and Flame, and Explosion Phenomena 3 (1948)
698 89-98.
699 [10] A.J. Morales, I.M. Lasky, M.K. Geikie, C.A. Engelmann, K.A. Ahmed, Mechanisms of
700 flame extinction and lean blowout of bluff body stabilized flames, Combust. Flame 203 (2019)
701 31-45.
702 [11] P. Strakey, T. Sidwell, J. Ontko, Investigation of the effects of hydrogen addition on lean
703 extinction in a swirl stabilized combustor, Proc. Combust. Inst. 31 (2007) 3173-3180.
704 [12] Y. Zhang, J. Wu, S. Ishizuka, Hydrogen addition effect on laminar burning velocity, flame
705 temperature and flame stability of a planar and a curved CH4–H2–air premixed flame, Int. J.
706 Hydrogen Energ. 34 (2009) 519-527.

[13] A. Liñán, M. Vera, A.L. Sánchez, Ignition, Liftoff, and Extinction of Gaseous Diffusion Flames, Annu. Rev. Fluid. Mech. 47 (2015) 293-314.

[14] A.P. Giles, R. Marsh, P.J. Bowen, A. Valera-Medina, Applicability of the Peclet number approach to blow-off and flashback limits of common steelworks process gases, Fuel 182 (2016) 531-540.

[15] L. Selle, T. Poinsot, B. Ferret, Experimental and numerical study of the accuracy of flame-speed measurements for methane/air combustion in a slot burner, Combust. Flame 158 (2011) 146-154.

[16] J. Fu, C. Tang, W. Jin, Z. Huang, Effect of preferential diffusion and flame stretch on flame structure and laminar burning velocity of syngas Bunsen flame using OH-PLIF, Int. J. Hydrogen Energ. 39 (2014) 12187-12193.

[17] J. Natarajan, T. Lieuwen, J. Seitzman, Laminar flame speeds of H2/CO mixtures: Effect of CO2 dilution, preheat temperature, and pressure, Combust. Flame 151 (2007) 104-119.

[18] T.M. Vu, M.S. Cha, B.J. Lee, S.H. Chung, Tip opening of premixed bunsen flames: Extinction with negative stretch and local Karlovitz number, Combust. Flame 162 (2015) 1614-1621.

[19] K.S. Kedia, A.F. Ghoniem, The blow-off mechanism of a bluff-body stabilized laminar premixed flame, Combust. Flame 162 (2015) 1304-1315.

[20] A.E. Dahoe, K. Hanjalic, B. Scarlett, Determination of the laminar burning velocity and the Markstein length of powder–air flames, Powder Technol. 122 (2002) 222-238.

[21] A.A. Konnov, A. Mohammad, V.R. Kishore, N.I. Kim, C. Prathap, S. Kumar, A comprehensive review of measurements and data analysis of laminar burning velocities for various fuel+air mixtures, Prog. Energy Combust. 68 (2018) 197-267.

[22] L.P.H. de Goey, A. van Maaren, R.M. Quax, Stabilization of Adiabatic Premixed Laminar Flames on a Flat Flame Burner, Combust. Sci. Technol. 92 (1993) 201-207.

[23] N.A. Malik, J.C. Fung, Anomalous burning rates of flamelets induced by self-similar multiple scale (fractal and spiral) initial fields, Phys. Rev. E 62 (2000) 6636-6647.

[24] S. Goroshin, M. Bidabadi, J.H.S. Lee, Quenching distance of laminar flame in aluminum dust clouds, Combust. Flame 105 (1996) 147-160.

[25] S.B. Sathe, R.E. Peck, T.W. Tong, Flame Stabilization and Multimode Heat Transfer in Inert Porous Media: A Numerical Study, Combust. Sci. Technol. 70 (1990) 93-109.

[26] A.J. Barra, G. Diepvens, J.L. Ellzey, M.R. Henneke, Numerical study of the effects of material properties on flame stabilization in a porous burner, Combust. Flame 134 (2003) 369-379.

[27] A.J. Barra, J.L. Ellzey, Heat recirculation and heat transfer in porous burners, Combust. Flame 137 (2004) 230-241.

[28] P. Habisreuther, F.C.C. Galeazzo, P. Chockalingam, N. Zarzalis, Structure of laminar premixed flames of methane near the auto-ignition limit, Combust. Flame 160 (2013) 2770-2782.

[29] Z. Chen, P. Dai, S. Chen, A model for the laminar flame speed of binary fuel blends and its application to methane/hydrogen mixtures, Int. J. Hydrogen Energ. 37 (2012) 10390-10396.

[30] S.L. Aly, C.E. Hermance, A Two-Dimensional Theory of Laminar Flame Quenching, Combust. Flame 40 (1981) 173-185.

[31] N. Weinberg, J.B. Greenberg, On Blow-Out and Lift-Off of Laminar Jet Diffusion Flames, Combust. Sci. Technol. 188 (2016) 1760-1776.

[32] Y.-C. Wu, Z. Chen, Asymptotic analysis of outwardly propagating spherical flames, Acta Mechanica Sinica 28 (2012) 359-366.

[33] G.H. Markstein, M.L. Polanyi, Flame Propagation - A Critical Review of Existing Theories, Report No. 61, Cornell Aeronaut Lab Inc., Buffalo, NY, 1947.

[34] E.V. Jithin, R.J. Varghese, R.K. Velamati, Experimental and numerical investigation on the effect of hydrogen addition and N2/CO2 dilution on laminar burning velocity of methane/oxygen mixtures, Int. J. Hydrogen Energ. 45 (2020) 16838-16850.

[35] R.-H. Chen, Z. Li, T.X. Phuoc, Propagation and stability characteristics of laminar lifted diffusion flame base, Combust. Flame 159 (2012) 1821-1831.

[36] J. Li, S.K. Chou, W.M. Yang, Z.W. Li, A numerical study on premixed micro-combustion of CH4–air mixture: Effects of combustor size, geometry and boundary conditions on flame temperature, Chem. Eng. 150 (2009) 213-222.

[37] A.A. Konnov, Yet another kinetic mechanism for hydrogen combustion, Combust. Flame 203 (2019) 14-22.

[38] E. Gimeno-Escobedo, A. Cubero, J.S. Ochoa, N. Fueyo, A reduced mechanism for the prediction of methane-hydrogen flames in cooktop burners, Int. J. Hydrogen Energ. 44 (2019) 27123-27140.

[39] N. Donohoe, A. Heufer, W.K. Metcalfe, H.J. Curran, M.L. Davis, O. Mathieu, D. Plichta, A. Morones, E.L. Petersen, F. Güthe, Ignition delay times, laminar flame speeds, and mechanism validation for natural gas/hydrogen blends at elevated pressures, Combust. Flame 161 (2014) 1432-1443.

[40] E. Salzano, G. Pio, A. Ricca, V. Palma, The effect of a hydrogen addition to the premixed flame structure of light alkanes, Fuel 234 (2018) 1064–1070.

[41] V. Di Sarli, A.D. Benedetto, Laminar burning velocity of hydrogen–methane/air premixed flames, Int. J. Hydrogen Energ. 32 (2007) 637-646.

[42] E.J.K. Nilsson, A. van Sprang, J. Larfeldt, A.A. Konnov, The comparative and combined effects of hydrogen addition on the laminar burning velocities of methane and its blends with ethane and propane, Fuel 189 (2017) 369–376.

780 [43] L. Xiang, H. Jiang, F. Ren, H. Chu, P. Wang, Numerical study of the physical and chemical
781 effects of hydrogen addition on laminar premixed combustion characteristics of methane and
782 ethane, Int. J. Hydrogen Energ. 45 (2020) 20501-20514.
783 [44] Y. He, Z. Wang, L. Yang, R. Whiddon, Z. Li, J. Zhou, K. Cen, Investigation of laminar
784 flame speeds of typical syngas using laser based Bunsen method and kinetic simulation, Fuel
785 95 (2012) 206-213.
786 [45] X. Hu, Q. Yu, J. Liu, N. Sun, Investigation of laminar flame speeds of CH4/O2/CO2
787 mixtures at ordinary pressure and kinetic simulation, Energy 70 (2014) 626-634.
788 [46] D.R. Jones, W.A. Al-Masry, Charles W. Dunnill, Hydrogen-enriched natural gas as a
789 domestic fuel: an analysis based on flash-back and blow-off limits for domestic natural gas
790 appliances within the UK, Sustainable Energy Fuels 2 (2018) 710-723.
791 [47] A. Hassanpouryouzband, E. Joonaki, K. Edlmann, N. Heinemann, Thermodynamic and
792 transport properties of hydrogen containing streams, Sci. Data 7 (2020) 222.
793 [48] D. Wang, C. Ji, S. Wang, H. Meng, Z. Wang, J. Yang, Further understanding the premixed
794 methane/hydrogen/air combustion by global reaction pathway analysis and sensitivity analysis,
795 Fuel 259 (2020) 116190.
796 [49] R. Gaudron, M. Gatti, C. Mirat, T. Schuller, Impact of the injector size on the transfer
797 functions of premixed laminar conical flames, Combust. Flame 179 (2017) 138-153.
798 [50] F.H.V. Coppens, J. De Ruyck, A.A. Konnov, Effects of hydrogen enrichment on adiabatic
799 burning velocity and NO formation in methane + air flames, Exp. Therm. Fluid Sci. 31 (2007)
800 437–444.
801 [51] C.-E. Lee, C.-H. Hwang, S.-C. Hong, Proposal and validation of a new type of flame
802 stability diagram for partially premixed flames, Fuel 87 (2008) 3687-3693.

803 [52] J.P. Szybist, K. Chakravathy, C.S. Daw, Analysis of the Impact of Selected Fuel
804 Thermochemical Properties on Internal Combustion Engine Efficiency, Energy Fuels 26
805 (2012) 2798−2810.
806 [53] R.A. Bonilla, N.R.L. Maccalum, Flame Stabilization on Rectangular Burners, Combust.
807 Flame 12 (1968) 492-498.
808 [54] F.G. Roper, The Prediction of Laminar Jet Diffusion Flame Sizes: Part I. Theoretical
809 Model, Combust. Flame 29 (1977) 219-226.
810 [55] W. Dai, C. Qin, Z. Chen, C. Tong, P. Liu, Experimental studies of flame stability limits
811 of biogas flame, Energy Convers. Manag. 63 (2012) 157-161.
812 [56] Y. Zhou, S. Peng, X. Huang, C. Wu, J. Zhang, LNG–Air Mixture as a Supplementary
813 Energy Injection into a Biogas Distribution Network, Energies 10 (2017) 1902.
814 [57] Y. Zhang, W. Gao, Y. Yu, M. Wang, C. Chen, Primary air ratio change and gas
815 interchangeability index correct for domestic gas cooker burning multi-source natural gases, J.
816 Nat. Gas. Sci. Eng. 35 (2016) 276-282.
817 [58] R.T.E. Hermanns, A.A. Konnov, R.J.M. Bastiaans, L.P.H. De Goey, K. Lucka, H. Köhne,
818 Effects of temperature and composition on the laminar burning velocity of CH4 +H2 +O2 +N2
819 flames, Fuel 89 (2010) 114–121.

820